A computer-aided diagnosis system for lung nodule detection in chest radiographs using a two-stage classification method based on radial gradient and template matching

Ryoichi Nagata, Tsuyoshi Kawaguchi
Faculty of Engineering
Oita University
Oita, Japan

Hidetoshi Miyake
Faculty of Medicine
Oita University
Yufu, Japan

***Abstract*—In this paper we propose a scheme for automated detection of lung nodules in chest radiographs. The proposed scheme first segments lungs in a chest image using an active shape model. Next, the scheme detects initial nodule candidates by using a method previously reported by the authors. After that, the proposed scheme classifies nodule candidates into nodules and false positives by using a two-stage classification method proposed in this paper. For performance evaluation of the proposed nodule detection scheme, we made experiments using 125 images with nodules in the JSRT database which is a public database. We created 40 data sets by 40 randomized selection of 80 training images and 45 test images from the 125 images. As the result of experiments using these 40 data sets, the proposed scheme gave 6.6, 7.6, and 9.1 false positives per image for sensitivity values of 60.1, 64.1, and 69.7% on the average of 40 data sets. The time needed by the proposed scheme was 8.2 seconds per image on the average of 40 data sets using 3.3GHz Intel PC.**

Keywords—computer-aided diagnosis; chest radiographs; nodule detection; false-positive reduction; template matching

I. INTRODUCTION

Detection of lung nodules is important for early detection and treatment of lung cancers. Chest radiography is currently the most frequently used screening procedure for lung cancer. However, studies show that radiologists fail to detect lung nodules in chest radiographs in as many as 30% of positive cases. Thus, computer-aided diagnosis (CAD) schemes have been developed to help to reduce false-negatives in the diagnoses of lung cancers using chest radiography [1-8].

The automated nodule detection technique has been considered to be one of the most promising CAD techniques for lung nodule detection in chest radiographs [1-8]. This technique consists of the following two steps : detection of initial nodule candidates in chest radiographs ; classification of the detected candidates into nodules and false positives. For classification of nodule candidates, many schemes used multilayer artificial neural networks (ANNs) trained by back-propagation [1-5]. Although only a few scheme was evaluated by public database, Coppini et al. [4] evaluated the performance of their ANN based scheme by the JSRT database [9] which is a public database. They reported that their scheme gave 4.3, 7.6, and 10.2 false positives per image for sensitivity values of 60, 70, and 75% as the result of experiments using 119 images with nodules in the JSRT database. However, ANNs trained by back-propagation have many parameters which have to be determined by trial and error and they may require an enormous amount of time for their training.

Several researchers employed non-ANN based classifiers for false-positive reduction [6-8]. Li et al. [6] used a template matching based classifier. Schilham et al. [7] employed a *k* nearest neighbor classifier. Hardie et al. [8] used a Fisher's linear discriminant classifier. The schemes of [7] and [8] gave the performance comparable to the ANN based scheme of [4] in the experiments using the JSRT database. In this paper we propose an automated nodule detection scheme using a two-stage classification method based on radial gradient and template matching.

II. DATA SETS

In the experiment, we use the JSRT database [9], which is a public database. The images in the JSRT database has a pixel size of 0.175 mm, a matrix size of 2048×2048, and a gray level range of 12 bits. We reduce the matrix size and the gray level range of the images to 512×512 and 8 bits, respectively. The pixel size of the reduced image is 0.7 mm. The JSRT database has 154 images with nodules and 93 images without nodules. And, the centroids and diameters of nodules are given for the 154 images with nodules. In addition, according to the degree of subtlety of the lung nodule, the 154 images with nodules are grouped into five levels of 1 (extremely subtle), 2 (very subtle), 3 (subtle), 4 (relatively obvious), and 5 (obvious). We use all

978-1-4799-2761-6/13/$31.00 ©2013 IEEE

images without nodules and 125 images with nodules of levels 1 to 4. The JSRT database has 142 images with nodules of levels 1 to 4. These 142 images include 17 images with nodules hidden by heart and structures below the diaphragm. According to [5], images with nodules hidden by the heart and structures below the diaphragm are excluded in our experiments.

III. The Proposed Nodule Detection Scheme

Figure 1 shows an application of the nodule detection scheme proposed in this paper. Figure 1(a) gives a chest image with a nodule which is marked by a circle. The proposed scheme first segments lungs using the lung segmentation algorithm proposed in this paper, which is an active shape model-based scheme and similar to the algorithm of [10] (Fig.1(b)). Next, the scheme detects nodule-candidate locations within the lung regions using the nodule-candidate detection scheme proposed in [11] (Fig.1(c)). After that, the proposed scheme classifies the nodule-candidate locations into nodules and false positives by using a two-stage classification method, which consists of the first and the second-stage classifiers (Figures 1(d) and (e)). Finally, the proposed scheme applies a hierarchical aggromerative clustering method to the candidate locations classified into nodules to determine the centers of the clusters as 'the centers of suspected areas of the nodules' (Fig.1(f)). In the remainder of this section, we show the details of the proposed scheme.

A. Lung segmentation

For automated lung segmentations, we employ an active shape model(ASM) and closely follow the method described in [10]. To train the ASM, we use the 93 images without nodules in the JSRT database. For each of the 93 training images, we first place 44 landmark points on the right lung boundary and 50 landmark points on the left lung boundary using the results shown in the SCR database [12].

Next, we automatically determine the lung top, the midline of thorax, and the lung length and width for each training image by using the method proposed in [13]. The method of [13] detects the lung top, the lung bottom, and the right and left ribcage boundaries in each chest image. We give the lung length by the distance between the lung top and the lung bottom and the lung width by the distance between the two intersection points at which the horizontal line equally distant from the lung top and the lung bottom intersects the right and left boundaries. The midline of thorax is given by the perpendicular bisector of the line segment connecting the two intersection points described above.

After detecting the lung top, the midline of thorax, and the lung length and width for each training image, we calculate the average lung length, L_a, and the average lung width, W_a, over all training images, and then we scale all of the training images in the x and y directions so that the scaled images have lung lengths and widths equal to L_a and W_a, respectively. After that, we give the coordinates of landmarks placed on the lung

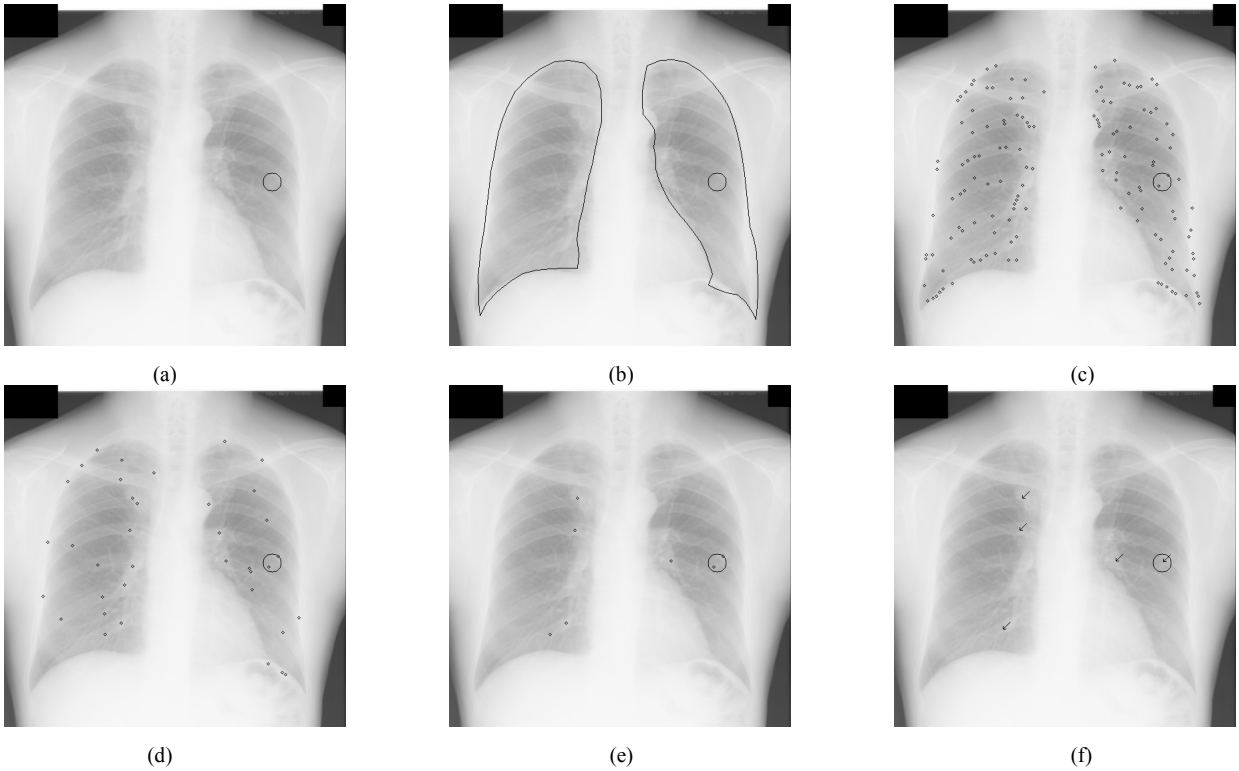

Fig. 1. An application of the proposed nodule detection scheme. (a) An original chest image in which a nodule is shown by a circle. (b) The lung regions obtained by the lung segmentation algorithm proposed in this paper. (c) The locations of nodule candidates obtained by the algorithm of [11]. (d) The locations of nodule candidate that were classified into nodules by the first-stage classifier. (e) The locations of nodule candidates that were classified into nodules by the second-stage classifier. (f) The centers of the clusters obtained by applying a hierarchical agglomerative clustering algorithm to the survived nodule candidates, which we determined as 'the centers of suspected areas of the nodules'.

boundaries in each training image by the coordinate system whose x and y-axes coincide with the lung top and the midline of thorax, respectively.

After normalizing lengths, widths, and positions of lungs in the training images by using the above method, we make an ASM for each of the right and left lungs. First, for each of the 93 training lungs, a shape vector is given by $(x_1, y_1, \cdots, x_n, y_n)^T$ where (x_1, y_1), $\cdots$, (x_n, y_n) are the landmark points placed on the boundary of the training lung. Note that n is 44 for the right lung and 50 for the left lung. Below, the shape vectors of the 93 training lungs are denoted by v_j, j = 1, $\cdots$, 93.

We apply principal component analysis to the shape vectors v_j. Let $\bar{v}$ denote the mean vector of v_j, j = 1, $\cdots$, 93. And, let λ_1, $\cdots$, λ_t be the t largest eigenvalues of the covariance matrix of v_j and φ_1, $\cdots$, φ_t be the eigenvectors corresponding to λ_1, $\cdots$, λ_t. Then, a lung shape is given by $v = \bar{v} + \Phi b$ where $\Phi = (\varphi_1, \cdots, \varphi_t)$ is the matrix of the first t eigenvectors and $b = (b_1, \cdots, b_t)$ is a vector of weights. In our experiments, t was set to 15 and b_i, i = 1, $\cdots$, 15, were constrained to lie within the range of $\pm 2\sqrt{\lambda_i}$.

To detect lungs in a test image, we first detect the lung top, the midline of thorax, and the lung length and width from the test image by using the same method as that employed in the modeling stage, and then we scale the test image in the x and y directions so that the scaled image has lung length and width equal to L_a and W_a, respectively. Next, the mean shape $\bar{v}$ is placed as an initial lung boundary in the scaled test image so as to superimpose the x and y-axes in the mean shape onto the lung top and the midline of thorax in the scaled test image. After that, we search a lung boundary with the minimum cost in the scaled test image by moving each landmark along the direction perpendicular to the contour. To calculate the cost of a lung boundary, we use a similar method to that described in [10].

B. Detection of Nodule Candidate Locations

After lung segmentation, we detect nodule-candidate locations within the lung regions using the nodule-candidate detection scheme proposed in [11]. The scheme first creates a nodule enhanced image from a chest image using the method of [4]. Next, the scheme places a square region with 448×448 matrix size on the nodule enhanced image in such a way that its central axis and its upper side are located on the midline of thorax and the lung top, respectively. After that, the square region is divided into 49 regions of interest(ROIs) with 64×64 matrix size as illustrated in Fig.2 (a). And then, for each of the 49 ROIs with 64×64 matrix size, a nodule search region with 128×128 matrix size having its central part with 64×64 matrix size corresponding to the ROI is located on the image as illustrated in Fig.2 (b). Nodule search regions are partially overlapped with adjacent ones in the image. The scheme of [11] detects nodule candidates within the intersection of each nodule search region and lung masks by employing multilevel thresholding. In this paper we use the centroids of the nodule candidates detected by the scheme of [11] as the nodule-candidate locations.

C. The first-stage classifier

The proposed nodule detection scheme classifies nodule candidates detected from a test image into nodules and false-positives by using the first and the second-stage classifiers. In the first-stage classifier, we first create a local-contrast image NI(x, y) from the test image I(x, y) by using the following operation :

$$NI(x,y) = \frac{I(x,y) - E(x,y)}{\left\{V(x,y) - (E(x,y))^2\right\}^{\frac{1}{2}}} \tag{1}$$

where E(x, y) and V(x, y) are the images obtained from I(x, y) and $(I(x, y))^2$ by applying the Gaussian filter with standard deviation of 16. The above operation was also used in [7] and [8]. Next, nodule candidates are segmented in the local-contrast image by using the segmentation algorithm of [8]. For each nodule candidate location (m, n), we give an average radial gradient (ARG) value at (m, n) by

$$ARG = \frac{1}{|A|} \sum_{(u,v)\in A} |g(u,v)| \times \cos(\theta(u,v)) \tag{2}$$

where A is the nodule candidate region corresponding to (m, n), |A| is the number of pixels in A, g(u, v) is the intensity gradient vector at pixel (u, v) in A, and θ(u, v) is the angle between the radial vector pointing from (u, v) to (m, n) and the gradient vector g(u, v). In the first-stage classifier, we select one-quarter of the nodule candidates detected from a test image in a non-increasing order of their ARG values to classify them into nodules.

D. The second-stage classifier

The second-stage classifier employs a template matching technique for classification of the nodule-candidate locations that were classified into nodules by the first-stage classifier. According to [6], we use 36×36 and 40×40 as the matrix sizes of templates and candidate images, respectively. The template matching technique proposed in this paper uses nodule templates and non-nodule templates in which nodules and non-nodules have an equal effective diameter. In addition, to calculate a similarity value between a nodule candidate detected in a test image and a template, the proposed technique scales the test image so that the effective diameter of

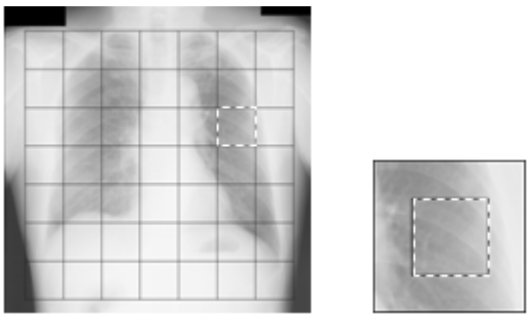

(a) (b)

Fig. 2. (a) 49 ROIs with size of 64×64 pixels located on a chest radiograph and (b) a nodule search region with size of 128×128 pixels.

the candidate becomes equal to that of the nodule (or the non-nodule) in the template.

First, we show the method used to create nodule templates. To evaluate the performance of the proposed nodule detection scheme, we use 40 data sets created from the 125 images with nodules in the JSRT database [9] by 40 different randomized selection of 45 test images and 80 training images. For each data set, we first create the right / left reversed image from each training image. Next, three images are made from each of the original and the reversed training image by performing three rotation and one scaling. Each training image is first rotated about its center by -10, 0, and 10 degrees and then scaled by factor of 20 / d where d is the diameter, represented in millimeters, of the nodule in the training image. After creating six images from each training image with the above method, we cut out a square block with size of 36×36 pixels centered at the centroid of the nodule from each of the six images to use it as a nodule template. Figure 3 shows a nodule template obtained by the above method. A circle with diameter of 20 mm centered at the centroid of the nodule is drawn in this figure.

Non-nodule templates are made from the 93 images without nodules in the JSRT database. We first perform the method of [11] on the 93 images to detect nodule candidates and then create non-nodule templates from the detected candidates. In the stage of detecting nodules from test images, nodule candidate images with 40×40 matrix size are made from nodule candidates detected in the test images. All candidate images are scaled to make the effective diameters of the candidates equal to 20 mm. The method that we employ to make non-nodule templates from nodule candidates is the same as that used for creating candidate images from nodule candidates detected in test images, except that non-nodule templates have matrix size of 36×36.

To classify a nodule-candidate location (m, n) detected in a test image, we first calculate the effective diameter of the nodule candidate region corresponding to (m, n), which has already been detected in the first-stage classifier. The effective diameter of a nodule candidate region is defined by the diameter of a circle having the same area as that of the candidate region. Next, we scale the test image to make the effective diameter of the candidate region equal to 20 mm (28.6 pixels). After that, we cut out a square block of 40×40 pixels centered at (m, n) from the scaled test image. Below, the square block is named as 'the candidate image centered at (m, n)'. Figure 4 shows a candidate image obtained by the above method. The second-stage classifier classifies a candidate location (m, n) by classifying the candidate image centered at (m, n).

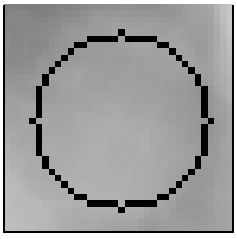

Fig. 3. A nodule template with matrix size of 36×36 created from a chest image after scaling to make the diameter of the nodule equal to 20mm (28.6 pixels).

To reduce the time needed for classification of candidate images, we prepare in advance the scaled-down templates of 9×9 pixels for all templates in the database. Below, we show the method used for classification of a candidate image. The size of the candidate image is first reduced to 10×10 pixels. Next, similarity values between the candidate image of 10×10 pixels and all templates of 9×9 pixels are calculated by using the template matching. To calculate the similarity value between a template A with size of 9×9 pixels and a candidate image B with size of 10×10 pixels, we move the template A inside the candidate image B in both horizontal and vertical directions, and the correlation value at each shift vector (s, t), s = 0 to 1 and t = 0 to 1, is calculated by the equation :

$$C(s,t) = \frac{\sum A(u,v)B(s+u,t+v)}{\left[\sum\{A(u,v)\}^2 \sum\{B(s+u,t+v)\}^2\right]^{\frac{1}{2}}} \qquad (3)$$

where Σ denotes the summation over all pixels (u, v) in the template A. The similarity value between the template A and the candidate image B is defined by the largest value of C(s, t) over all shift vectors (s, t), s = 0 to 1 and t = 0 to 1.

After calculating similarity values between the scaled-down candidate image and all scaled-down templates, we select 1000 templates in a non-increasing order of the similarity values. If all of the selected 1000 templates are non-nodule templates, the candidate image is determined to be a false positive. Otherwise, we compute similarity values between the candidate image of the original size and the templates of the original sizes corresponding to the selected 1000 templates and then give a discriminant function value, R, by

$$R = d_b / d_a, \quad d_a = \left(1 - a^2\right)^{\frac{1}{2}}, \quad d_b = \left(1 - b^2\right)^{\frac{1}{2}} \qquad (4)$$

where a is the largest similarity value over all nodule templates included in the 1000 templates and b is the largest similarity value over all non-nodule templates included in the 1000 templates. d_a and d_b are named as the distances of the candidate image to the nearest nodule template and to the nearest non-nodule template. The candidate image is determined to be a

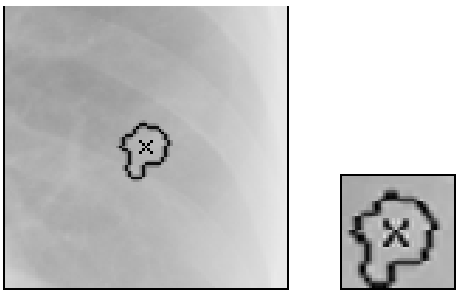

(a) (b)

Fig. 4. (a) A nodule candidate region, which was obtained by applying the segmentation algorithm of [8] to a nodule candidate detected by the method of [11]. (b) The nodule candidate image with matrix size of 40×40 created from the nodule candidate region as shown in Fig.4(a), after scaling to make the effective diameter of the candidate region equal to 20mm (28.6 pixels).

nodule if R > β for a threshold β, and otherwise it is determined to be a false positive.

E. Clustering of nodule candidates

The proposed scheme employs a hierarchical aggromerative clustering method [14] for the set of candidate locations that were classified into nodules by the second-stage classier. We give the distance between two clusters by the most distant pair of samples, one in each cluster. When the number of nodule candidates is K, the scheme initially creates K clusters, each of which consists of one candidate. Next, the scheme searches for the nearest pair of clusters and merges them, and reduce the number of clusters by 1. The scheme repeats the above procedure while the distance between the nearest pair of clusters is smaller than or equal to a threshold T_d. In the experiment, T_d was set to 24 mm which was the same value as the threshold that we used for judgement of whether or not the center of a suspected area of a nodule obtained by the proposed scheme was close enough to the centroid of the nodule. When we use the above clustering method, the distance between the most distant pair of candidates in each cluster becomes smaller than or equal to T_d. After clustering the nodule candidates, the proposed scheme gives the center of each cluster by the average of the centroids of candidates belonging to the cluster, and the center of each cluster is determined as "the center of a suspected area of the nodule".

IV. EXPERIMENTAL RESULTS

We first evaluated the performance of the lung segmentation algorithm proposed in this paper, the nodule-candidate detection scheme reported in [11], and the first-stage classifier using the 125 images with nodules in the JSRT database [9] that we showed in Section II. The lung segmentation algorithm could correctly segment lungs for all images, except one (JPCLN36). The nodule-candidate detection scheme, which created 142 nodule candidates per image, missed no nodules in the 124 images for which lungs could be successfully segmented. The first-stage classifier missed twelve nodules in the 124 images. The number of nodule candidates survived after application of the first-stage classifier was 37 per image on the average of the 124 images.

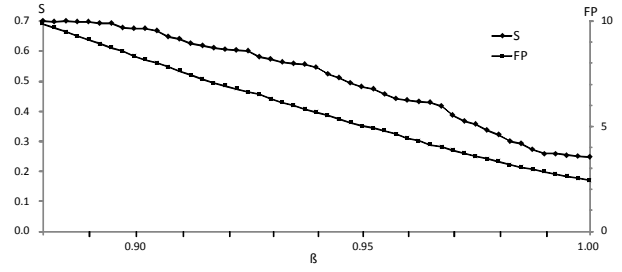

Fig. 5. A result obtained by performance evaluation of the proposed nodule detection scheme. The horizontal axis represents the threshold β. The left vertical axis denotes the sensitivity value, S, and the right vertical axis represents the average number of false positives per image, FP.

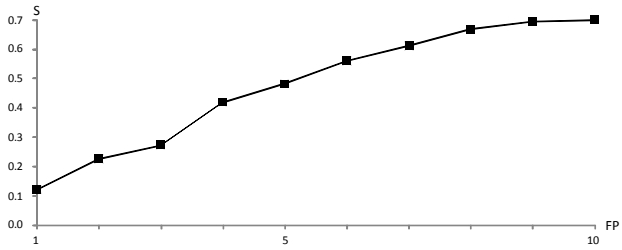

Fig.6. The free-response receiver operating characteristic (FROC) curve obtained from the result of Fig.5. The horizontal and vertical axes represent the average number of false positives per image, FP, and the sensitivity value, S, respectively.

Next, we evaluated the total performance of the automated nodule detection scheme proposed in this paper by the sensitivity value and the average number of false positives per image. Sensitivity is defined by the ratio of the number of nodules detected in the test images by the proposed scheme to the total number of nodules in the test images. Each of the 125 images with nodules used in the experiment has just one nodule. Thus, we defined sensitivity by the ratio of the number of test images with nodules successfully detected by the proposed scheme to the total number of test images.

The 93 images without nodules in the JSRT database [9] were used for training images of non-nodules. The 125 images with nodules in the JSRT database were used for both sets of training images for nodules and test images. From the 125 images with nodules in the JSRT database, we created 40 data sets by 40 different randomized selection of 45 test images and 80 training images for nodules. As shown above, the 125 images include thirteen images for which nodules have been missed before application of the second-stage classifier. We randomly selected 45 test images from the set of all 125 images including these thirteen images. The number of nodule templates was 480 and the number of non-nodule templates was 12690. The performance of the proposed scheme was evaluated by changing the threshold β on the discriminant function value R in the range of 0.8 to 1.0 at intervals of 0.025. According to [5], we judged that the proposed scheme could detect a nodule when the distance between the centroid of the nodule and the center of a suspected area of the nodule obtained by the proposed scheme was smaller than or equal to 24 mm.

Figure 5 shows the result of the experiment. In Fig.5, the horizontal axis represents the threshold β. The left vertical axis denotes the sensitivity values, S, and the right vertical axis represents the average number of false positives per image, FP. The values of S and FP shown in Fig.5 were obtained by averaging the values obtained for 40 data sets. Figure 6 shows the free-response receiver operating characteristic (FROC) curve obtained from the result of Fig.5 by plotting the sensitivity value against FP. In particular, for sensitivity values of 60.1, 64.1, and 69.7%, FP was 6.6, 7.6, and 9.1, respectively.

V. CONCLUSIONS

In this paper we proposed a scheme for automated detection of lung nodules in chest radiographs. The scheme first segments lungs in a chest image using the lung segmentation algorithm proposed in this paper, which is an active shape model-based algorithm. Next, the scheme detects nodule candidates within the lung regions using the method of [11]. After that, the scheme classifies the nodule candidates

into nodules and false positives by using a two-stage classification method proposed in this paper. For performance evaluation of the proposed scheme, we created 40 data sets by 40 randomized selection of 45 test images and 80 training images from the 125 images with nodules in the JSRT database. As the result of experiments using these 40 data sets, the proposed scheme gave 6.6, 7.6, and 9.1 false positives per image for sensitivity values of 60.1, 64.1, and 69.7% on the average of 40 data sets. The time needed by the proposed scheme was 8.2 seconds per image on the average of 40 data sets using 3.3 GHz Intel PC.

In [11], the authors proposed a nodule detection scheme for chest radiographs using a template matching-based classifier. The performance of the proposed scheme is superior to that of the scheme of [11] although the latter manually segments lung fields. The scheme of [11] gave 9.5 and 12.5 false positives per image for sensitivity values of 60.2 and 69.8%. It uses only template matching for false-positive reduction. In addition, the template matching technique used in [11] is different from that employed in this paper. To calculate a similarity values between a nodule candidate detected in a test image and a nodule template, the proposed scheme scales the test image so that the effective diameter of the candidate becomes equal to the diameter of the nodule in the nodule template. On the other hand, the scheme of [11] does not use such scaling. Instead, it creates in advance 26 scaled nodule templates from an original nodule template by using scales $S_j = (5+j) / d$, $j = 0, \cdots, 25$, where d is the diameter, represented in millimeters, of the nodule in the original nodule template.

The proposed scheme gave a slightly lower performance than the schemes of [7] and [8]. However, the proposed scheme needs only three features of each nodule candidate for its classification into a nodule and a false positive, which are the ARG value of the candidate and the distances of the candidate to the nearest nodule template and to the nearest non-nodule template. On the other hand, the schemes of [7] and [8] use 109 and 46 features of each nodule candidate. In addition, these scheme require selection of an optimal subset of features for each set of training images and for each level of specificity.

REFERENCES

[1] J. S. Lin, S. C. B. Lo, A. Hasegawa, M. T. Freedman, and S. K. Mun, "Reduction of false positives in lung nodule detection using a two-level neural classification," IEEE Trans. Medical Imaging, vol.15, no.2, pp. 206–217, 1996.

[2] M. G. Penedo, M. J. Carreira, A. Mosquera, and D. Cabello, "Computer-aided diagnosis : A neural-network-based approach to lung nodule detection," IEEE Trans. Medical Imaging, vol. 17, no. 6, pp. 872–880, 1998.

[3] B. Keserci and H. Yoshida, "Computerized detection of pulmonary nodules in chest radiographs based on morphological features and wavelet snake model," Medical Image Analysis, vol. 6, pp. 431–447, 2002.

[4] G. Coppini, S. Diciotti, M. Falchini, N. Villari, and G. Valli, "Neural networks for computer-aided diagnosis : Detection of lung nodules in chest radiograms," IEEE Trans. Information Technology in Biomedicine, vol. 7, no. 4, pp. 344–357, 2003.

[5] J. Shiraishi, Q. Li, K. Suzuki, R. Engelmann, and K.Doi, "Computer-aided diagnostic scheme for the detection of lung nodules on chest radiographs : Localized search method based on anatomical classification," Med. Phys., vol.33, no. 7, pp. 2642–2653, 2006.

[6] Q. Li, S. Katsuragawa, and K. Doi, "Computer-aided diagnostic scheme for lung nodule detection in digital chest radiographs by use of a multiple-template matching technique," Med. Phys., vol. 28, no. 10, pp. 2070–2076, 2001.

[7] A. M. R. Schilham, B. van Ginneken, and M. Loog, "A computer-aided diagnosis system for detection of lung nodules in chest radiographs with an evaluation on a public database," Medical Image Analysis, vol.10, pp. 247-258, 2006.

[8] R. C. Hardie, S. K. Rogers, T. Wilson, and A. Rogers, "Performance analysis of a new computer aided detection system for identifying lung nodules on chest radiographs," Medical Image Analysis, vol.12, pp. 240-258, 2008.

[9] J. Shiraishi, S. Katsuragawa, J. Ikezoe, T. Matsumoto, T. Kobayashi, K. Komatsu, M. Matsui, H. Fujita, Y. Kodera, and K. Doi, "Development of a digital image database for chest radiographs with and without a lung nodule : receiver operating characteristic analysis of radiologists' detection of pulmonary nodules," American Journal of Roentgenology, vol. 174, pp. 71–74, 2000.

[10] B. van Ginneken, A. F. Frangi, J. J. Staal, B. M. ter Haar Romeny, and M. A. Viergever, "Active shape model segmentation with optimal features," IEEE Trans. Medical Imaging, vol. 21, no. 8, pp. 924–933, 2002.

[11] R. Nagata, T. Kawaguchi, and H. Miyake, "Automated detection of lung nodules in chest radiographs using a false-positive reduction scheme based on template matching," Proc. 5th Int. Conf. Biomedical Engineering and Infomatics, pp.216-223, 2012.

[12] B. van Ginneken, M. B. Stegmann, and M. Loog, "Segmentation of anatomical structures in chest radiographs using supervised methods : a comparative study on a public database," Medical Image Analysis, vol.10, pp.19-40, 2006.

[13] R. Nagata, T. Kawaguchi, and H. Miyake, "Accurate detemination of lung boundary from lung apex to costophrenic angle in chest radiographs," Proc. 2nd Int. Conf. Biomedical Engineering and Infomatics, vol.1, pp.86-91, 2009.

[14] K. C. Gowda and G. Krishna, "Agglomerative clustering using the concept of mutual nearest neighbourhood," Pattern Recognition, vol. 10, no. 2, pp. 105–112, 1978.